A new kinematic–dispersive wave van Genuchten (KDW-VG) model for numerical simulation of preferential water flow in soil

Mostafa Moradzadeh, Saeed Boroomandnasab, Hadi Moazed, Javad Alavi, Ali Jamalian, Mohammadreza Khaledian, Stéphane Ruy

A New Kinematic–Dispersive Wave van Genuchten (KDW-VG) Model for Numerical Simulation of Preferential Water Flow in Soil

Mostafa Moradzadeh[a,*] Saeed Boroomandnasab[a] Hadi Moazed[a] Javad Alavi[b] Ali Jamalian[c] Mohammadreza Khaledian[d] Stéphane Ruy[e]

[a] **Department of Irrigation and Drainage Engineering, Faculty of Water Sciences Engineering, Shahid Chamran University of Ahvaz, Ahvaz, Khuzestan, Iran**

[b] **Department of Applied Mathematics, School of Mathematical Sciences, University of Guilan, P.O. Box 1914, Rasht 41938, Iran**

[c] **Department of Computer Sciences, Faculty of Mathematical Sciences, University of Guilan, Rasht, Iran**

[d] **Department of Water Engineering, Faculty of Agricultural Sciences, University of Guilan, Rasht, Guilan, and Department of Water Engineering and Environment, Caspian Sea Basin Research Center, Iran**

[e] **Avignon Université, INRAE, EMMAH, F-84000, Avignon, France**

* Corresponding author. Department of Irrigation and Drainage Engineering, Faculty of Water Sciences Engineering, Shahid Chamran University of Ahvaz, Ahvaz, Khuzestan, Iran. Tel: +989017126240; Fax: +986133365670.

E-mail address: moradzadeh.mostafa@gmail.com (M. Moradzadeh).

Abstract

Preferential water flow in soil macropores such as underground channels formed by worm activity and plant root growth, can move a large volume of water and contaminants

to groundwater resources in a short time. To describe these types of water flow in soil, Di Pietro et al. (2003) developed and proposed kinematic–dispersive wave (KDW) model. They suggested this model by adding a dispersive term to the kinematic wave (KW) model that was severely convective and was presented by Germann in 1985. The fundamental assumption of this model is that the water flux (u) is exclusively a function of the mobile water content, but in the KDW model, considering its additional dispersive term, it is assumed that the water flux is a non-linear function of the mobile water content and its first-time derivative. The first term of this assumption is a power function where the water flux depends on the mobile water content. This equation is just a mathematical equation and has no significant physical meaning. In this research, this power function is substituted by the shape of van Genuchten model that has an acceptable physical meaning, and thus the kinematic–dispersive wave van Genuchten (KDW-VG) model is introduced for the first time as the innovation of this research. The models were calibrated and validated with observations of four different rainfall intensities that were applied on the surface of a soil column with artificial preferential pathways. The output water fluxes from the bottom of the soil column versus the soil mobile volumetric water content in the column were recorded at set times. First, both the KDW and KDW-VG models were calibrated and their indefinite coefficients were determined by minimizing the error function between the observed and modelled water fluxes versus mobile volumetric water content using particle swarm optimization (PSO) algorithm. Next, both models, which are second-degree non-linear partial differential equations, were solved using numerical finite difference method with the MATLAB programming language, and were validated by experimental observations of rainfall hydrograph that was passed through the preferential routes of a physical model and was recorded from the bottom of the soil

column. Root-mean-square error (RMSE) comparison of the models predictions and observations indicated that the proposed model (KDW-VG) could predict the observations more accurately compared with the KDW model, and also had better performance in the calibration stage.

Keywords: Preferential water flow, Artificial preferential pathways, Porous media, Numerical solution, Particle swarm optimization (PSO) algorithm, Finite difference

Introduction

Preferential water flow which is a non-uniform flow, is a common phenomenon in unsaturated soils. This type of flow normally causes the rapid movement of pollutants and is often observed when mass transport is dominated by macropore flow (Sheng et al., 2011; Li et al., 2018; Cohen and Weisbrod, 2018). Flows through macropores are a kind of preferential flow that occur on paths created by earthworms or plant roots (Gerke., 2006; Khitrov et al., 2009; Klammler et al., 2017). Blue dye tracer studies show that the tracer moves not only along cracks but also through the burrows created by earthworms (Sander and Gerke, 2007). The appearance of preferential paths has been confirmed by direct observation using sequential magnetic resonance imaging (MRI) (Hoffman et al., 1996). The occurrence of this phenomenon during water infiltration depends on the initial water content of soils, the amount and intensity of rainfall, and soil hydraulic conductivity (Jarvis, 2007). Studies show that deep water movement in soils is predominantly due to the existence of preferential flow paths (Alaoui, 2015). In non-homogeneous and cracked soils, water flows move significantly faster than the soil matrix (Snehota et al., 2015) and create numerous splits in the soil profile,

resulting in poor water retention (Alaoui, 2015) and influencing runoff regulation, sediment transportation, and soil and water conservation (Tao, 2017). Solutes such as nitrogenous fertilizer and phosphorus that are widely used in agriculture (Moradzadeh et al., 2014) are transported through these routes and thereby, contaminate both surface and underground water (Flury, 1996; Zhang et al., 2017; Saadat et al., 2018), indirectly affecting the amount and concentration of runoff salts. Preferential flows induced by macropores are the main cause of pollution transport and groundwater circulation and contamination. Chemical fertilizers can also easily be transported through soil macropores to groundwater (Zhang et al., 2015). Therefore, preferential flows can have a significant effect on human life, products, and ecology (Niu et al., 2007).

Investigation of the behaviour of contaminant transport in the soil matrix requires knowledge of the equations governing water movement in the soil. Additionally, further research appears necessary to understand the enhancement of contaminant transport by preferential paths (Majdalani et al., 2008). In this regard, Germann (1985, 1990) and Chen and Wagenet (1992) extracted the relationship between average water flux (u) and mobile water content in draining porosity (Germann., 1985; Germann., 1990; Chen and Wagenet., 1992). Both models revealed a non-linear relationship between water flux and the amount of mobile water content. These equations, which are based on the law of continuity, finally lead to the kinematic wave (KW) model to simulate preferential water flow, but usually overestimate the real flows (Germann, 1985; Di Pietro et al., 2003). As the

KW model is severely convective, it cannot consider the dispersive effect, because this model assumes that water flux is just a function of mobile water content (Di Pietro et al., 2003). To compensate for this defect, the kinematic–dispersive wave (KDW) model was proposed by Di Pietro and colleagues in 2003 to simulate preferential water flows in draining porosity with more accuracy (Di Pietro et al., 2003; Majdalani et al., 2008). In this model, a dispersive term was added to the KW model and it was assumed that the water flux was a non-linear function of the mobile water content, and its first time derivative. This improvement made the KDW model more accurate than the KW model. The first term of this assumption is a power function where the water flux depends on mobile water content and the second term is a differential equation that models the hysteresis water content effect in the soil matrix. The power function term is just a mathematical equation and has no significant physical meaning. In this study, this power function is replaced with the shape of van Genuchten model that is more physically based. As the primary contribution of the study, the kinematic–dispersive wave van Genuchten (KDW-VG) model is introduced for the first time, which is the innovation of this research.

Definition of models

Kinematic–dispersive wave (KDW) model

To apply the KDW model (Di Pietro et al., 2003), some fundamental assumptions listed by Di Pietro et al. (2003) and Niu et al. (2007) should be considered. The most important assumption is that the gravitational force dominates the capillary force and the other forces are not considered in the system. Therefore, the flow

transport is assumed to have a vertical downward direction. The other important assumption states that the model is established principally in the mobile water section. Given these assumptions, w is the mobile volumetric water content, $w_t = \partial w/\partial t$ is the first-order partial time derivative of w, and u is the volumetric water flux. This assumes that the microporosity is completely saturated, so there is no water exchange between the two porosities. The law of continuity equation and its first derivative with respect to z are respectively defined as (Di Pietro et al., 2003):

$$\frac{\partial w(z,t)}{\partial t} + \frac{\partial u(z,t)}{\partial z} = 0 \quad (1)$$

$$\frac{\partial^2 w(z,t)}{\partial z \partial t} + \frac{\partial^2 u(z,t)}{\partial z^2} = 0 \quad (2)$$

It is also assumed that the volumetric water flux within the macropores is a non-linear function of the relation between w and w_t, described by the following equation:

$$u = u(w, w_t) \Rightarrow u(z,t) = b[w(z,t)]^a \pm \nu_w \frac{\partial w(z,t)}{\partial t} \quad (3)$$

Accordingly, in the same water content, the negative sign is applied when the volumetric water flux of the drainage stage is greater than that of infiltration, and the positive sign is used when the volumetric water flux of infiltration stage is greater than that of drainage. Because, as will be explained later, the results of this study showed that, in the same water content, the volumetric water flux of the infiltration stage would be greater than drainage, the positive sign is used to define the formula. The model depends on three coefficients, where $u(z,t)$ [mm h^{-1}] is volumetric water flux in time t and depth z, a is a macropore-flow distribution

index, b [mm h^{-1}], is a conductance term, and v_w [mm] is the water dispersion coefficient, all of which are positive numbers (Majdalani et al., 2008).

Given the first derivative of Eq. (3) with respect to z, the following description is derived:

$$\frac{\partial u}{\partial z} = \frac{\partial u}{\partial w} \cdot \frac{\partial w}{\partial z} + \frac{\partial u}{\partial w_t} \cdot \frac{\partial w_t}{\partial z} \Rightarrow \frac{\partial u(z,t)}{\partial z} = ab[w(z,t)]^{a-1} \frac{\partial w(z,t)}{\partial z} + v_w \frac{\partial^2 w(z,t)}{\partial z \partial t} \quad (4)$$

where $c(w) = \left.\frac{\partial u(z,t)}{\partial w}\right|_{w_t=\text{constant}} = ab[w(z,t)]^{a-1}$ is signal speed and v_w is equal to $\left.\frac{\partial u(z,t)}{\partial w_t}\right|_{w=\text{constant}}$.

The continuity equation, Eq. (1), and Eq. (4) are combined to give the following equation:

$$\frac{\partial w(z,t)}{\partial t} + ab[w(z,t)]^{a-1} \frac{\partial w(z,t)}{\partial z} = -v_w \frac{\partial^2 w(z,t)}{\partial z \partial t} \quad (5)$$

Considering the first derivative of the continuity equation, Eq. (2), the following equation is derived from the substitution of $\partial^2 w(z,t)/\partial z \partial t = -\partial^2 u(z,t)/\partial z^2$ and multiplication of $\partial u(z,t)/\partial w$ or $ab[w(z,t)]^{a-1}$ on both sides of Eq. (5):

$$\frac{\partial u(z,t)}{\partial t} + ab[w(z,t)]^{a-1} \frac{\partial u(z,t)}{\partial z} = v_w ab[w(z,t)]^{a-1} \frac{\partial^2 u(z,t)}{\partial z^2} \quad (6)$$

Neglecting the second term of Eq. (3), $\pm v_w \cdot \partial w(z,t)/\partial t$, $w(z,t) = (u(z,t)/b)^{\frac{1}{a}}$ is derived. Finally, with the substitution of $(u(z,t)/b)^{\frac{1}{a}}$ instead of $w(z,t)$, the following non-linear partial differential equation was derived by Di Pietro and colleagues in 2003 (Majdalani et al., 2008):

$$\frac{\partial u(z,t)}{\partial t} + ab^{\frac{1}{a}}[u(z,t)]^{\frac{a-1}{a}}\frac{\partial u(z,t)}{\partial z} = \nu_w ab^{\frac{1}{a}}[u(z,t)]^{\frac{a-1}{a}}\frac{\partial^2 u(z,t)}{\partial z^2} \quad (7)$$

Model development

Modified KDW model with combination of van Genuchten model– Introducing the kinematic–dispersive wave van Genuchten (KDW-VG) model

As mentioned, Di Pietro and colleagues in 2003 applied Eq. (3) to model volumetric water flux. In this equation, $\pm\nu_w \cdot \partial w(z,t)/\partial t$ is the term that can model the loops of the hysteresis phenomenon during the infiltration–drainage cycles, and $b[w(z,t)]^a$ is a power function that appears to have been taken from the power form of the volumetric water flux versus mobile water content (Fig. 1), as reported by Di Pietro and colleagues in 2003.

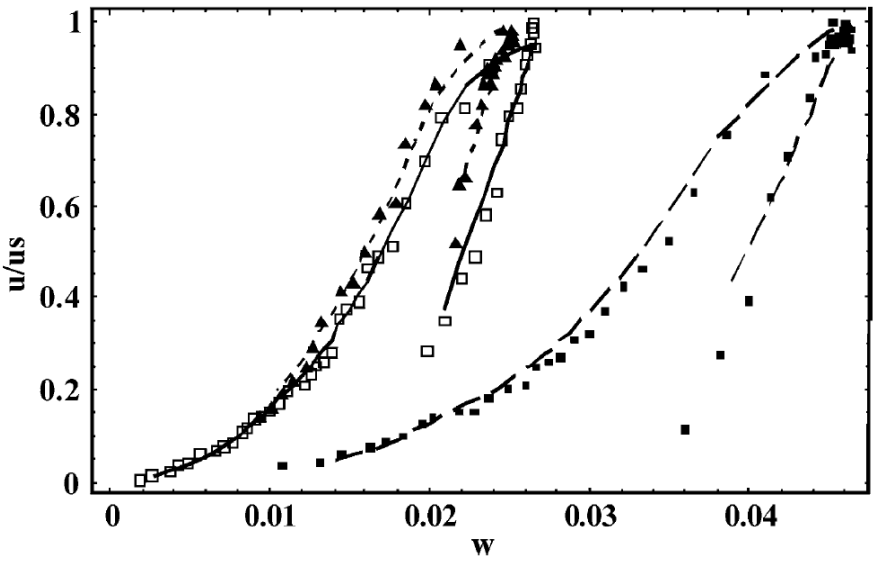

Fig. 1. Relative flux (u/u_s) versus mobile water content for three input intensities (u_s). Symbols show measured water fluxes and lines show fitted values to Eq. 3 (Di Pietro et al., 2003)*.

As Fig. 1 shows, the curves follow a form of the power equation which is an empirical model. The power function term of Eq. (3), $b[w(z,t)]^a$, emphasizes the mathematical aspects with fewer physical assumptions. Here, this term is substituted with the van Genuchten model, which is more physically based. van Genuchten in 1980 showed that, based on the theory of Mualem's capillary model (Mualem, 1976), the hydraulic conductivity model can be expressed in closed form (Radcliffe and Simunek, 2010).

van Genuchten model

The van Genuchten equation (van Genuchten, 1980; Abbasi et al., 2012; Wang et al., 2017) is an unsaturated hydraulic conductivity equation that has a physical base and is presented as follows:

$$K(S_\mathrm{e}) = K_\mathrm{s} {S_\mathrm{e}}^{l} \left(1 - \left(1 - {S_\mathrm{e}}^{\frac{1}{m}}\right)^{m}\right)^2, m = 1 - \frac{1}{n}, n > 1 \quad (8)$$

$$S_e = \frac{w - w_r}{w_s - w_r} \quad (9)$$

where S_e [-] is the effective water content, $K(S_\mathrm{e})$ and K_s [L T^{-1}] are the unsaturated and saturated hydraulic conductivity, respectively, l is the pore connectivity value, n and m are dimensionless empirical constants, w [L^3 L^{-3}] is the soil volumetric

* Fig 1 was reprinted from Elsevier, 278 (1-4), Liliana Di Pietro, Stephane Ruy, Yvan Capowiez, Predicting preferential water flow in soils by traveling-dispersive waves, Page 70, Copyright (2003), with permission from Elsevier, License Number: 4396440670492.

185 water content, w_r is the residual soil volumetric water content, and w_s is the
186 saturated or field-saturated soil volumetric water content. As the volumetric water
187 flux resembles hydraulic conductivity in terms of physical and dimensions, and
188 similarly, its amount varies between different levels of water content, here the
189 apparent shape of the van Genuchten model is used instead of the first term of Eq.
190 (3), $b[w(z,t)]^a$. According to the experimental conditions, some slight variations
191 should be applied to the definitions of the input parameters of the van Genuchten
192 model. Whereas the amount of S_e is normalized and dimensionless, in this study
193 with the redefinition of the parameters of S_e as w_min and w_max, the amount of S_e
194 always varies between 0 and 1. Instead of w_r, w_min is substituted in as the minimum
195 amount of soil volumetric water content due to rainfall in each data series, and w_s
196 is substituted with w_max as the maximum amount of observed water content in
197 each experiment. Therefore, with the redefinition of the parameters of S_e, $S_e{}^*$ is
198 defined as $(w(z,t) - w_{min})/(w_{max} - w_{min})$. In this study, all experiments were
199 conducted in the unsaturated condition, and w_{max} denotes the maximum amount
200 of water content due to rainfall and is related to the maximum amount of water flux
201 in each experiment. Therefore, we changed w_r and w_s to w_{min} and w_max,
202 respectively. Both the van Genuchten model and the first term of Eq. (3),
203 $(b[w(z,t)]^a)$, are power functions, but the van Genuchten model has more
204 significant physical meaning. In the proposed model, the first term of Eq. (3),
205 $(b[w(z,t)]^a)$, is substituted with the van Genuchten model.

Thus, with the general format of the van Genuchten model for simulating water flux and considering the hysteresis term of Eq. (3), $\pm v_w \cdot \partial w(z,t)/\partial t$, the following equation is derived:

$$u(z,t) = u_{in}({S_e}^*)^l \left(1 - \left[1 - ({S_e}^*)^{\frac{1}{m}}\right]^m\right)^2 \pm v_w \frac{\partial w(z,t)}{\partial t} \quad (10)$$

As mentioned previously, the value of c in the KDW model is: $\left.\frac{\partial u}{\partial w}\right|_{w_t=\text{constant}}$. Thus, the first derivative of Eq. (10) will be as follows:

$$c(w) = \left.\frac{\partial u}{\partial w}\right|_{w_t=constant}$$

$$= \frac{l \times u_{in}(w(z,t) - w_{min})^{l-1}}{(w_{max} - w_{min})^l} \times \left(1 - \left[1 - ({S_e}^*)^{\frac{1}{m}}\right]^m\right)^2$$

$$+ \frac{2u_{in}}{w_{max} - w_{min}} \left(1 - \left[1 - ({S_e}^*)^{\frac{1}{m}}\right]^m\right) \times \left(1 - ({S_e}^*)^{\frac{1}{m}}\right)^{m-1} \times ({S_e}^*)^{\frac{1}{m}+l-1}$$

(11)

Therefore, after defining all parameters of the KDW-VG model, the model is introduced as below:

$$\frac{\partial u(z,t)}{\partial t} + c(u)\frac{\partial u(z,t)}{\partial z} = v_u \frac{\partial^2 u(z,t)}{\partial z^2} \quad (12)$$

where $v_u = c(u) \cdot v_w$.

To solve Eq. (12) numerically, $c(u)$ should be specified. For the KDW model, this was solved as mentioned by the substitution of $w(z,t) = (u(z,t)/b)^{\frac{1}{a}}$ into $c(w) = \left.\frac{\partial u}{\partial w}\right|_{w_t=constant} = ab[w(z,t)]^{a-1}$, and the expression for w was arranged

according to u. Here, for the sake of simplicity, Di Pietro did not consider the hysteresis term of Eq. 3, $(\pm v_w \cdot \partial w(z,t)/\partial t)$, to be eligible to easily arrange the expression for w according to u. Otherwise, algebraically, it would not be possible to create this change in the variable. This can partly hinder the convergence of the equation to better results.

However, in the KDW-VG model, to consider the full relationship between the observed values of w and u, a numerical relationship was created between these two terms, and then the function of $w = f(u)$ was considered as a polynomial using the least-squares method. In this way, the effect of hysteresis water content was also considered. In this study, Eqs. (7) and (12) are solved in the MATLAB programming language by the finite-difference method, and with the following initial and boundary conditions, which were used by Germann in 1985:

$$\begin{cases} u(z,t) = u_{\text{in}}(t), z = 0, t > 0 \\ u(z,t) = u_0, z > 0, t = 0 \end{cases} \quad (13)$$

where $u_{\text{in}}(t)$ is the initial water flux.

Estimation of coefficients of both models

The indefinite parameters of both models are defined by minimizing the error function of the root-mean-square error (RMSE) between the observed and modelled water fluxes (Eqs. (3) and (10)) versus mobile water content.

In the KDW model, the parameters a, b, and v_w are unknown. These parameters are defined by the following equation:

$$RMSE = \sqrt{\frac{1}{N}\sum_{i=1}^{N}\left(u_i - \left(bw_i^a \pm v_w \frac{\partial w}{\partial t}|_i\right)\right)^2} \quad (14)$$

where N, u_i, and w_i are the number of experimental observations, observed fluxes at the bottom of the soil column at time i, and mean measured mobile water content at time i, respectively.

In addition, in the KDW-VG model, the indefinite parameters l, m, and v_w are calculated using the following equation:

$$RMSE = \sqrt{\frac{1}{N}\sum_{i=1}^{N}\left(u_i - \left[u_{in}\left(\frac{w_i - w_{min}}{w_{max} - w_{min}}\right)^{l}\left(1 - \left[1 - \left(\frac{w_i - w_{min}}{w_{max} - w_{min}}\right)^{\frac{1}{m}}\right]^{m}\right)^{2} \pm v_w \frac{\partial w}{\partial t}|_i\right]\right)^{2}} \quad (15)$$

To define the indefinite parameters of the two above mentioned models, the amount of RMSE in Eqs. (14) and (15) should be minimized. For this minimization, the heuristic method of particle swarm optimization (PSO) (Salahi et al., 2013) is applied in the present work.

Finally, both KDW and KDW-VG models, represented by Eqs. (7) and (12) respectively, are solved using the finite difference method and the models are validated. In other words, the hydrograph of drainage from the bottom of the soil columns due to an artificial rainfall, is compared with the results of the KDW and KDW-VG models in corresponding water fluxes. It is hypothesized that the proposed model will provide a better prediction of the observations due to more physical assumptions in the KDW-VG model based on Mualem's (1976) capillary model. Overall, the main objectives of this study are to (1) estimate the preferential water flow parameters of both KDW and KDW-VG models to achieve the global

minimum of error function using the PSO algorithm, and (2) validate both models with experimental observations to compare their performance.

Optimization

One of the most important aspects of this study is to estimate the parameters of applied models by finding the global minimum of the error functions. As the model developed in this study (KDW-VG) is an innovation of the research, the ranges of the model parameters are not definite, except for parameter m, which varies between 0 and 1. Therefore, this research is the first attempt to optimize and determine the parameters of the model, with the aim of minimising the error function. The literature review also shows that the KDW model has seldom been used to explain preferential water flow behavior and so far, its parameters have rarely been estimated by inverse methods (local or global). Therefore, the variation range of the parameter is still unclear, and this can be attributed to the occurrence of the local optimization problem. This study is one of the first attempts to optimize the parameters of the KDW model. The study attempts to find the global minimum of the error functions. Global methods have the advantage of avoiding the problems of local optimizations. However, this advantage is obtained through a large number of evaluations of the objective function (Rauch and Harremoës, 1999). As the parameters of the applied models are obtained by the PSO algorithm, the features of this method are briefly presented.

Particle swarm optimization (PSO) algorithm

PSO is one of the optimization methods inspired by nature and has been designed to solve numerical optimization problems (NOP) with a very large search space and without the need to know the gradient of the objective function. This method was first introduced by Kennedy and Eberhart (1995). The method is a suitable way to find the optimal global point of an error function (Tsoulos and Stavrakoudis., 2010). In this algorithm, to solve an optimization problem, a population of candidate responses randomly flows into the scope of the problem using a simple relation, and then it is explored to find the optimal global answer.

Algorithm operation

Assume that X, the search space for the PSO algorithm, is an n-dimensional and continuous search space. Each particle in the t-repetition of the PSO algorithm has three attributes: $x(t)$, the current position of the particle in the t-repetition; $v(t)$, the current speed of the particle in the t-repetition; and $y(t)$, the best individual position of the particle until t-repetition. The suitability of each particle is equal to its objective function value. Then, each particle moves in the search space with an initial speed of v, based on the suitability of the particle and other particles in the group. The best individual position of the particle until t-repetition yields the $y(t)$ that is the best value and the best position of the particle from the beginning to the t-repetition. Now it is easy to determine $y_i(t)$, that is, the best individual position of the particle i until t-repetition, based on the following relation:

$$y_i(t) = \begin{cases} x_i(t) & F(x_i(t)) < F(y_i(t-1)) \\ y_i(t-1) & o.w. \end{cases} \quad (16)$$

In the above equation, the function F is the value of the suitability of each particle based on the objective function. After definition of $y_i(t)$, the set of $P(t)$ can be defined as follows:

$$P(t) = \{y_1(t), y_2(t), \ldots, y_m(t)\} \quad (17)$$

Subsequently, for the minimization mode, $\hat{y}(t)$, which is the best global position found between all particles of the group until t-repetition, is defined as:

$$\hat{y}(t) = y_g(t) = \underset{i=1,\ldots,m}{\operatorname{argmin}} \quad F(y_i(t)) \quad (18)$$

Then, the position of each particle can be updated at the end of each iteration based on the following relations:

$$v_i^{t+1} = \omega v_i^t + r_1 c_1 (y_i^t - x_i^t) + r_2 c_2 (\hat{y}_t - x_i^t) \quad (19)$$

$$x_i^{t+1} = x_i^t + v_i^{t+1} \quad (20)$$

where r_1, $r_2 \sim U(0,1)$ represent uniformly distributed random numbers that are applied to maintain the dispersion of the particles and induction of the random property of particle motion, and prevent them from sudden mutation. c_1 and c_2 are individual and social acceleration coefficients that control the personal and global best values, respectively, and their values are determined by trial and error based on empirical results. To start the optimization, these numbers are usually considered to be around 2. On the other hand, $r_1 c_1 (y_i^t - x_i^t)$ is the personal component that determines the rate of efficiency of particle i relative to the previous steps, and $r_2 c_2 (\hat{y}_t - x_i^t)$ is the global (social) component that determines the efficiency rate of the particle i relative to the whole group. In Eq. (19), the

inertia weight ω, actually provides a relation for the particle speed that allows for more efficient search in the search space. Regarding Eq. (19), it is obvious that, large values of ω lead to a global search (i.e., a large-step search) and small values of ω lead to a local search (i.e., a small-step search). Therefore, with the application of large values of ω, the algorithm will regularly search for new spaces without as much focus on accurate local searches, while by reducing the values of ω, the search will be performed more locally and around the optimal answers obtained in the previous generation. Many relationships have already been proposed to determine the inertia weight (see Shi and Eberhart, 1998; Eberhart and Shi, 2001; Malik et al., 2007; Feng et al., 2007; Nikabadi and Ebadzadeh, 2008; Kentzoglanakis and Poole, 2009; Li and Gao, 2009; Chen et al., 2018; Yan et al., 2018; Ajdad et al., 2019).

Materials and methods

Laboratory and numerical studies were conducted to investigate the preferential water flow in artificial macropores under different rainfall intensities. An artificial preferential path was made by inserting a light soil lens into a field soil matrix, which is proven to have a considerable effect on the preferential water flow. To find an appropriate soil for the experiments, different soil samples were first studied. The samples were oven-dried at 105 °C for 24 h and passed through a 2 mm stainless steel screen. Then, the hydraulic conductivity of the soil samples was measured by the constant pressure head method. After selecting the appropriate soil to construct the model, the main sample, which had an artificial preferential

path to simulate the preferred water flow in the soil (created by coarse sand), was prepared using the following procedure (Wang et al., 2013, 2014). First, a PVC tube with an internal diameter of 15.5 cm and a height of 40 cm was prepared. The bottom of the soil column was covered with a double layer of plastic mesh with a pore diameter of 1–2 mm. Sharp-edge sand was also glued to the inner wall of the PVC tube, to increase the friction of the walls against the soil and reduce the probability of preferential flows from the walls. Then, about 1 cm of gravel (between the two sieves No. 10 and No. 6 (2 and 3.35 mm, respectively)) was poured onto the plastic mesh for better drainage. Next, the empty PVC tube with a tripod was placed in a bucket of water, which was filled with water to about one-third of the height of the soil column. A tube with an external diameter of 1.4 cm and a height of 60 cm was placed in the center of the PVC tube temporarily. Subsequently, the soil was slowly poured into the PVC tube around the inner tube. After pouring the soil around the inner tube at each stage, the water was drained from the bottom by gravity and the soil was allowed to almost dry. After this, the inner tube was carefully pulled out from the PVC tube without disturbing the surrounding main experimental soil, leaving a 1.4 cm diameter hole in the center of the main column. The hole was immediately filled with coarse sand. To avoid the collapse of the hole walls as the inner tube was pulled out of the middle of the main PVC tube, the whole soil column was filled by wet pack method in three successive steps. In each step, a length of 10 cm was filled (Wang et al., 2013, 2014). At the end of each step, the hole that was considered for creating the macropores was

371 carefully filled with light sand. This was repeated three times until the entire soil
372 sample was finally added. The soil had a coefficient of uniformity, C_u, of 1.645, a
373 coefficient of curvature, C_c, of 1.183, and a median grain size (D_{50}) of 0.146 mm.
374 The particle diameters of the coarse sand used to fill the inner hole were between
375 0.85 and 1 mm. After the construction of the soil sample, the saturated hydraulic
376 conductivity of the whole soil sample was measured by the constant pressure head
377 method as 172.6 mm h^{-1}. Then the soil column was made saturated from the
378 bottom for 48 h before the infiltration–drainage experiments. After saturation of
379 the soil column, the water was allowed to be drained by gravity until the weight of
380 the soil column was stabilized. After ensuring the emptying of soil pores involved
381 in the preferential flow, mostly macropores, the soil column was most probably
382 kept moist by water retained by capillary forces in micropores. A little exchange of
383 water is expected between micropores and drainage porosity. The amount of
384 water in the micropores could be determined by weighing the soil column. Then,
385 as shown in Fig. 2, a funnel was attached to the bottom of the soil column.

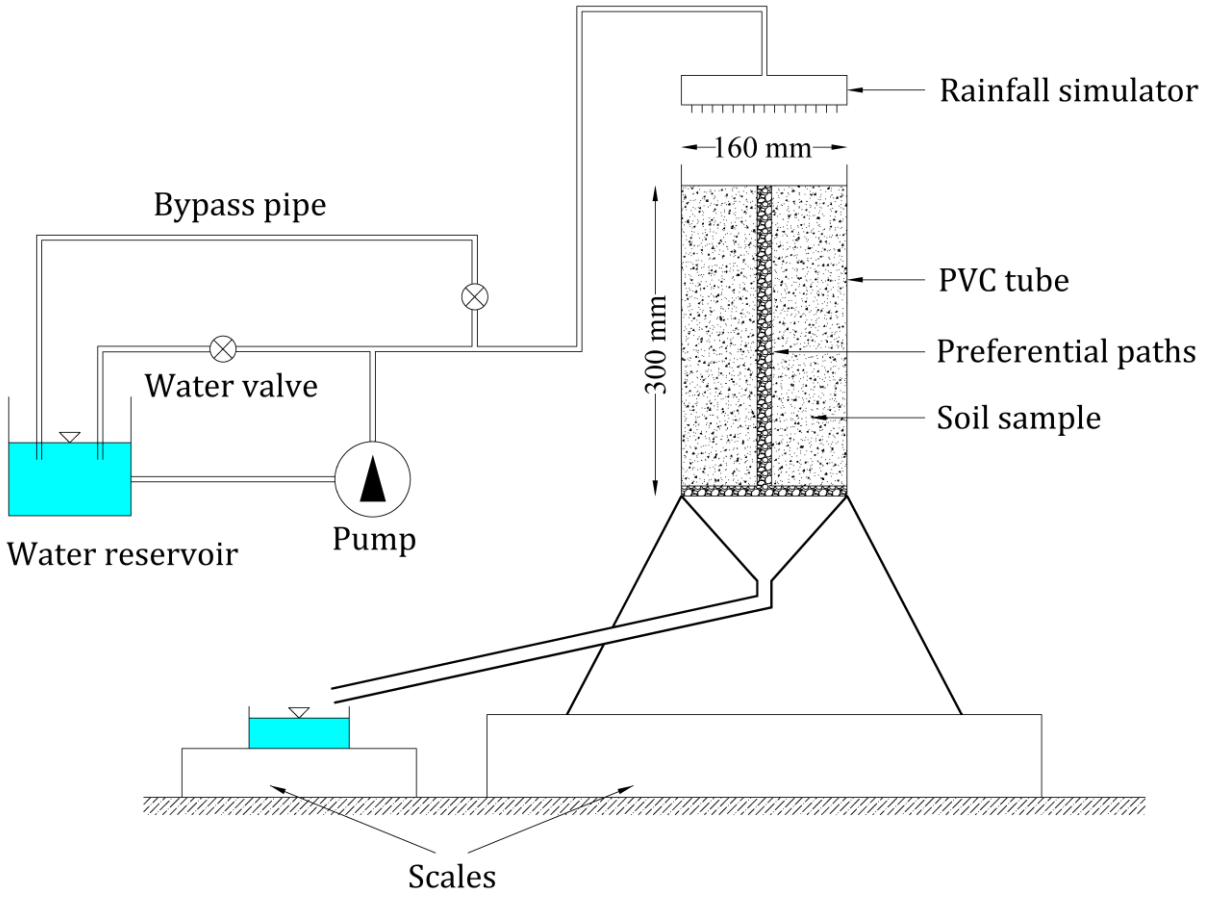

Fig. 2. Experimental setup of the infiltration–drainage experiments.

After preparing the soil sample and the physical model, as shown in Fig. 2, water droplets were created on the surface of the soil column with a rainfall simulator located about 10 cm above the soil surface. The rainfall simulator was connected to a pump fed from a water tank (Majdalani et al., 2008). The pump and two bypass pipes controlled rainfall duration and intensity. The flow condition was unsaturated, and the rainfall intensities should not have exceeded the hydraulic conductivity of the whole soil sample. The drainage flow was also monitored continuously with a precise scale, and the drainage hydrograph (water flux versus time) was derived from these data for each experiment. The larger scale was used to record the weight of the entire soil column moisture during the whole

experiment, to calculate the evaluation of the mobile soil water content of the soil column. The soil mobile volumetric water content at the desired time was calculated as follows:

$$w = \frac{M_{w-total} - M_{w-micropore}}{M_s} \times \rho_b \quad (21)$$

where w is the mobile volumetric water content, $M_{w-total}$ is the total mass of water stored into the soil column, $M_{w-micropore}$ is the mass of water stored in the micropores, M_s is the dry soil mass measured at the end of the experiments after oven drying at 105 °C, and ρ_b is the dry bulk density of the soil, given by the following equation:

$$\rho_b = \frac{M_s}{V_t} \quad (22)$$

where V_t is the total volume of the soil column. For this study, the dry bulk density was 1.47 g cm^{-3}.

In this study, infiltration experiments were performed with four simulated rainfall intensities of 56.97, 107.64, 133.01, and 161.71 mm h^{-1}. Two different scales were used. One was set at the bottom of the funnel to determine the amount of drainage flow, and the other was used to weigh the whole soil sample. Thus, as soon as the second scale reached a plateau, the rainfall simulator could be switched off. From this point, the scale placed under the funnel recorded the drainage flow or the falling limb of the drainage hydrograph. The scale below the soil sample measured the amount of mobile water content at each moment, and the other scale measured the drainage flow at the bottom of the soil column.

Results and discussion

Calibration of the KDW and KDW-VG models

To determine the indefinite coefficients of both models, the objective functions, Eqs. (14) and (15), were minimized using the PSO algorithm for the KDW and KDW-VG models, respectively. The water flux (u) was drawn as a function of w in infiltration–drainage cycles in each of the four rainfall intensities (Fig. 3). This figure is similar to the findings of Di Pietro and colleagues in 2003, and shows a hysteresis loop between the infiltration and drainage stage. However, the direction of the hysteresis loop is different. In our experiments, the water flux was higher for the infiltration stage than for the drainage stage for a given soil water content. Therefore, the differential equation used in Eqs. (14) and (15) should have a positive sign. Di Pietro et al. (2003) found a negative sign in their equation as they observed that the water flux was lower for the infiltration stage than for the drainage stage. Different studies have reported contradictory results (Di Pietro et al., 2003; van Genuchten, 1980; Gallage et al., 2013; Nielsen and Biggar, 1961; Topp and Miller, 1966; Youngs, 1964; Poulovassilis, 1969). These authors used different soil textures in their research and achieved different results for the movement direction of the hysteresis cycle of soil moisture against the water flux. It seems that no general findings on the direction of the hysteresis loop can be drawn from the literature.

For each level of rainfall intensity, Eqs. (14) and (15) were fitted for the KDW and KDW-VG models to the observations plotted on Fig. 3.

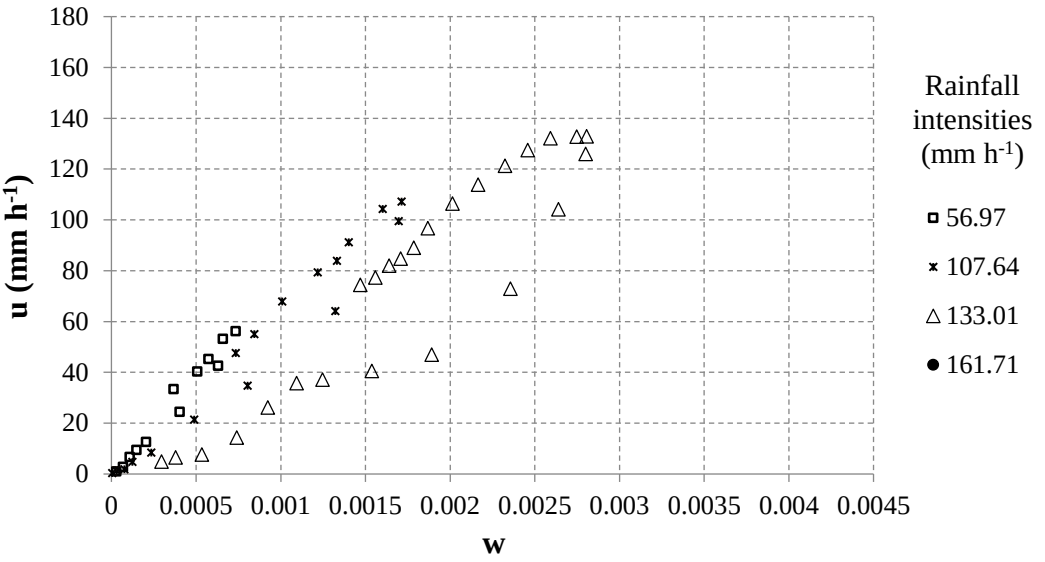

441

442 **Fig. 3. Water flux exiting the soil column at different rainfall intensities versus soil mobile**
443 **volumetric water content.**

444 In this study, for optimization, after investigating several relationships, the
445 relationship of linearly decreasing inertia weight presented by Xin et al. (2009)
446 was finally used to determine the inertia weight as follows:

447 $$\omega_k = \omega_{max} - \frac{\omega_{max}-\omega_{min}}{iter_{max}} \times k \qquad (23)$$

448 where ω_k is the amount of inertia weight in the k-repetition, and $\omega_{\min}$ and $\omega_{\max}$
449 are the amounts of inertia weight that are considered by default in this relationship
450 for the initial minimum and maximum values. Here, the values of 0.2 and 1.2 were
451 selected for $\omega_{\min}$ and $\omega_{\max}$, respectively, which yielded the best results, and the
452 maximum allowed iteration was the termination criterion of the optimization
453 algorithm. The initial value of ω_k was selected as 1 for the first generation and, due
454 to the values of $\omega_{\min}$ and $\omega_{\max}$, the number of created generations, and algorithm
455 iteration, after 5000 iterations this fell linearly to reach its minimum amount of 0.2.

This range of changes was selected by conducting calculations and reviewing previous studies (Bansal et al., 2011). Here, to make a balance between global and local searches and, therefore, faster convergence of the algorithm to the optimal global solution, the inertia weight was reduced uniformly throughout the implementation of the algorithm. In addition, according to Eq. (19), different values for c_1 and c_2 were selected and tested and, finally, the values of 1.2 and 2.4 for c_1 and c_2, respectively, yielded the best answers. Moreover, the size of each answer group, or the number of particles of each generation, in other words, the group size (m) in this study, were selected to be equal to 200 particles.

Calibration results of the KDW model and determination of indefinite coefficients of the model

Parameters a, b, and v_w were estimated according to Eq. (14), by minimizing the difference between the response of the relation of $b[w(z,t)]^a + v_w \cdot \partial w(z,t)/\partial t$ with u measured from the end of the soil column in corresponding w determined from the average whole of the soil column by the PSO algorithm. The optimization process of Eq. (14) and how to achieve the best results is shown in Fig. 4. The figure depicts the process of finding the optimal global point of the error function using the PSO algorithm for different rainfall intensities. Here, the horizontal axis represents the number of optimization algorithm iterations, and the vertical axis represents the value of the error function, which is equal to the RMSE of Eq. (14) computed for each iteration.

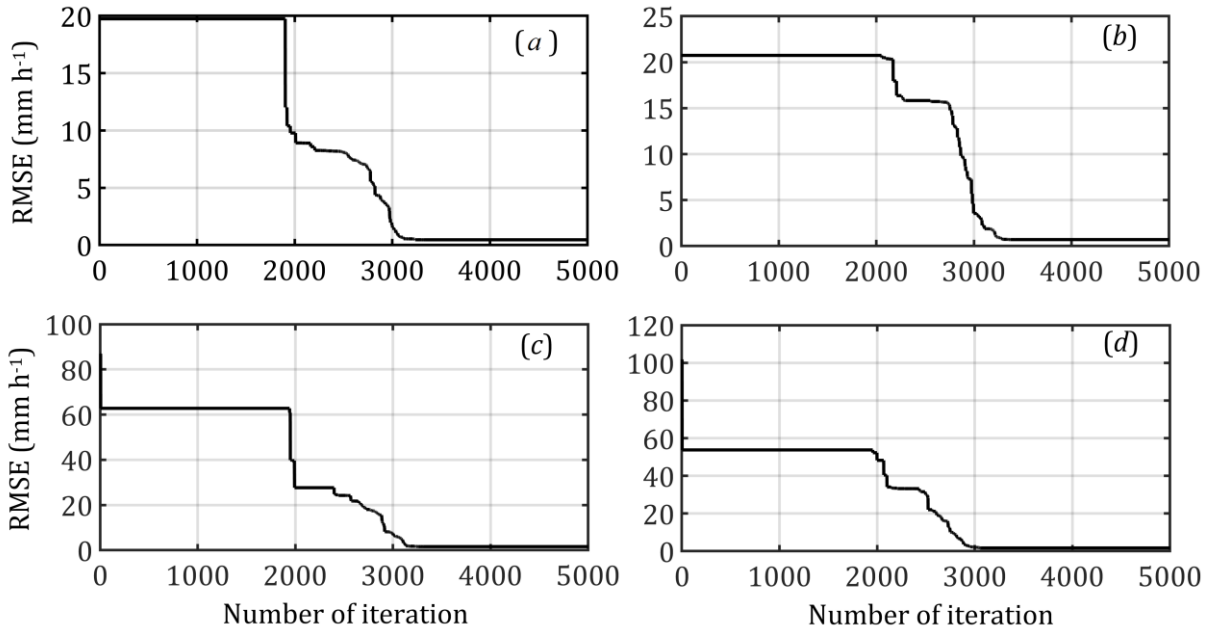

Fig. 4. Route finding of the optimal point of the objective function using the PSO algorithm, for the KDW model. a, b, c, and d represent the experiments with rainfall intensities of 56.97, 107.64, 133.01, and161.71 mm h^{-1}, respectively.

As can be seen in Fig. 4, the algorithm finds the best response whatever the rainfall intensity after about 3300 iterations, and the line becomes perfectly horizontal, reflecting a constant and minimum value of RMSE. The optimized coefficients of the KDW model are presented in Table 1.

Table 1 Optimized and calibrated coefficients of the KDW model for different rainfall intensities.

Rainfall intensity (mm h^{-1})	a	b (mm h^{-1})	v_w (mm)	RMSE (mm h^{-1})
56.97	1.0372	100076	90.55	0.46
107.64	1.0246	72095	89.26	0.70
133.01	1.0350	57058	89.41	1.60
161.71	1.0200	42062	90.64	1.71

The value of the parameter b decreases with an increase in rainfall intensity. Similar results were found by Di Pietro and Lafolie (1991) with the KW model on artificial soil, but contradictory results were found by Di Pietro et al. (2003) on natural soil with the KDW model. The macropore networks in Di Pietro et al. (2003) were formed by earthworms and were mainly cylindrical, whereas the macropore network in Di Pietro and Lafolie (1991) is quite similar to our experimental design due to the packing of large soil aggregates (mean diameter about 10 mm). The contradiction of our results with those of Di Pietro et al. (2003) can be related to the fact that in Di Pietro's research in 2003, at a constant moisture level, the amount of water flux in the drainage stage was higher than in the infiltration stage. We derived the opposite finding. The inconsistency in the direction of the hysteresis cycle movement may be associated with the difference in the applied soil texture in the two studies. Nonetheless, v_w was approximately constant. Moreover, the values of the parameter a were approximately 1. However, further experiments are needed to prove this trend. The results of the model fitting to the experimental observations are presented in Fig. 5, where the line depicts the fitted values of the model and the squares represent the observed values.

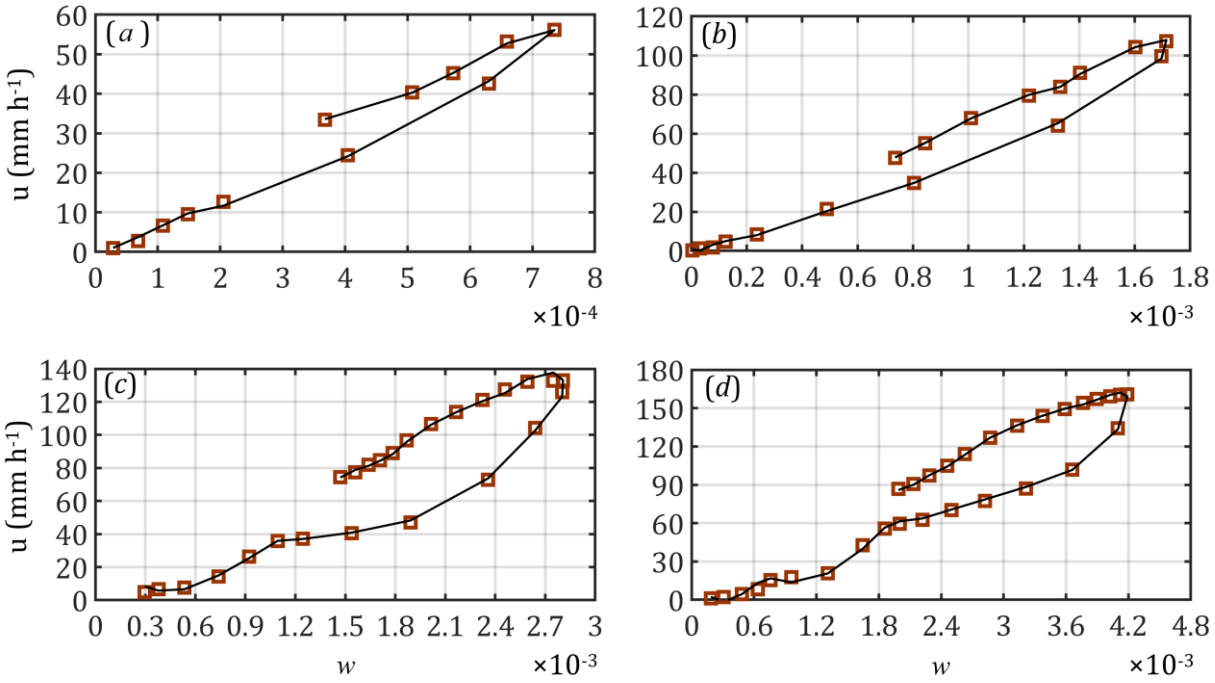

Fig. 5. Modelled and observed water flux exiting the soil column at different rainfall intensities versus soil mobile volumetric water content, for the KDW model. *a*, *b*, *c*, and *d* represent the experiments with rainfall intensities of 56.97, 107.64, 133.01, and161.71 mm h^{-1}, respectively.

As shown in Fig. 5, Eq. (14) fits the experimental observations well.

Calibration results of the KDW-VG model and determination of indefinite coefficients of the model

Again, to determine the indefinite coefficients of the model, the objective function was minimized using the PSO algorithm. Hence, the parameters l, m, and v_w were estimated with respect to Eq. (15) by minimizing the difference between the response of the relation of

$$u_{in}\left(\frac{w(z,t)-w_{min}}{w_{max}-w_{min}}\right)^{l}\left(1-\left[1-\left(\frac{w(z,t)-w_{min}}{w_{max}-w_{min}}\right)^{\frac{1}{m}}\right]^{m}\right)^{2}+v_w\frac{\partial w(z,t)}{\partial t}$$

with the u measured at the bottom of the soil column in corresponding w that was obtained from the average of the whole soil column. Fig. 6 displays the process of

achieving the best responses and optimization of Eq. (15) using the PSO algorithm for all different rainfall intensities. Here, the horizontal axis represents the number of optimization algorithm iterations, and the vertical axis represents the value of the error function, which is equal to the RMSE of Eq. (15) computed for each iteration.

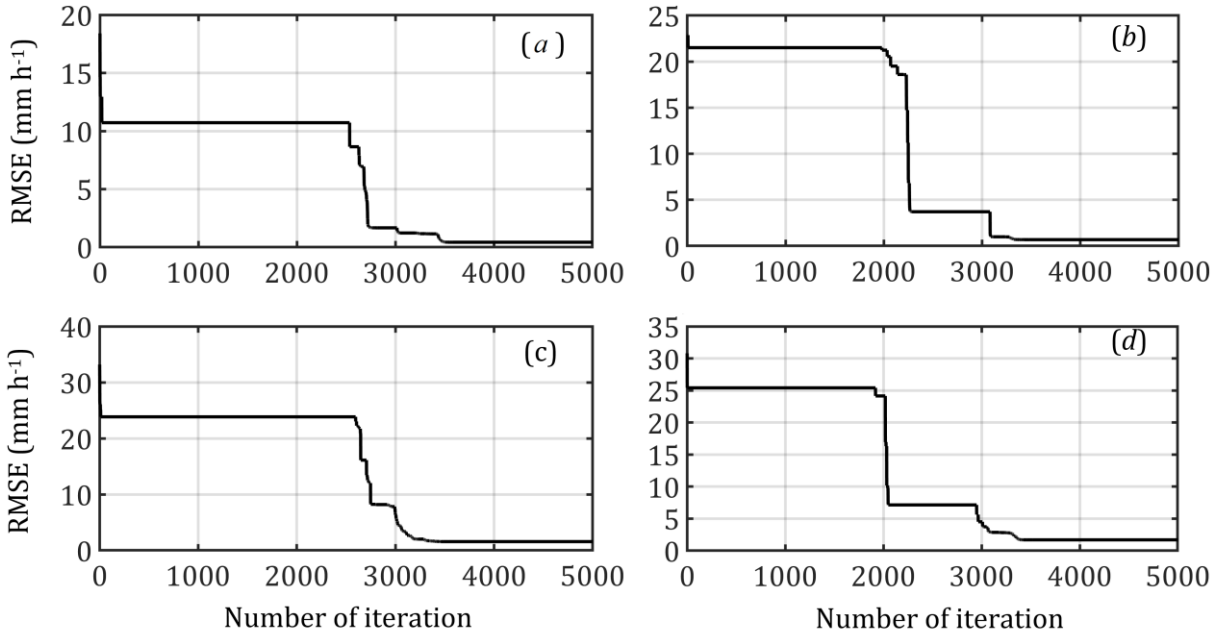

Fig. 6. Route finding of the optimal point of the objective function using the PSO algorithm, for the KDW-VG model. a, b, c, and d represent the experiments with rainfall intensities of 56.97, 107.64, 133.01, and161.71 mm h^{-1}, respectively.

Based on Fig. 6, the algorithm achieved the best response after 3500 iterations whatever the rainfall intensity, and the line became perfectly horizontal, reflecting a constant and minimum value of RMSE. The optimized coefficients of the KDW-VG model are presented in Table 2.

Table 2 Optimized and calibrated coefficients of the KDW-VG model for different rainfall intensities.

Rainfall intensity (mm h^{-1})	l	m	ν_w (mm)	RMSE (mm h^{-1})

56.97	-1.0458	0.9856	90.13	0.43
107.64	-1.0345	0.9847	89.81	0.68
133.01	-1.0494	0.9889	89.20	1.56
161.71	-1.0334	0.9863	90.90	1.70

532

533 We observe that, as the intensity was increased, the values of parameters l, m, and
534 v_w did not significantly change. This means that the ranges of the coefficients in the
535 model developed in this study are not sensitive to the intensity of input rainfall. In
536 the van Genuchten model, the value of m cannot be greater than 1, and higher
537 values of m represent more rapid movement of water or lighter texture of the soil.
538 In this regard, in an attempt to determine the coefficient m in the van Genuchten
539 model, Ghanbarian-Alavijeh et al. (2010) obtained the maximum amount of this
540 coefficient for the lightest soil (sand) as 0.61. Carsel and Parrish (1988) reported a
541 value of 0.63 for the coefficient m in sandy soil. This was 0.68 for sandy soil based
542 on the Rosetta database (Schaap et al., 2001). In addition, Leij et al. (1996) obtained
543 a maximum value of 0.85 for m in the van Genuchten model in sandy soil. Yates et
544 al. (1992) examined several types of sandy soil and reported that m and l in the
545 van Genuchten model were equal to 0.86 and -1.92, 0.85 and -1.3, and 0.84 and -
546 1.26, respectively. These values imply that due to the existence of preferential
547 flows in the current study and the rapid movement of water through macropores,
548 the value of 0.98 that was derived for m in the present study seems logical.

Conversely, according to Table 2, the values of l obtained in this study are approximately equal to the values reported by Yates (Yates et al., 1992). The results of model fitting to the experimental observations are shown in Fig. 7. Here, the squares represent the observed values and the line is the fitted value of the model to the observation.

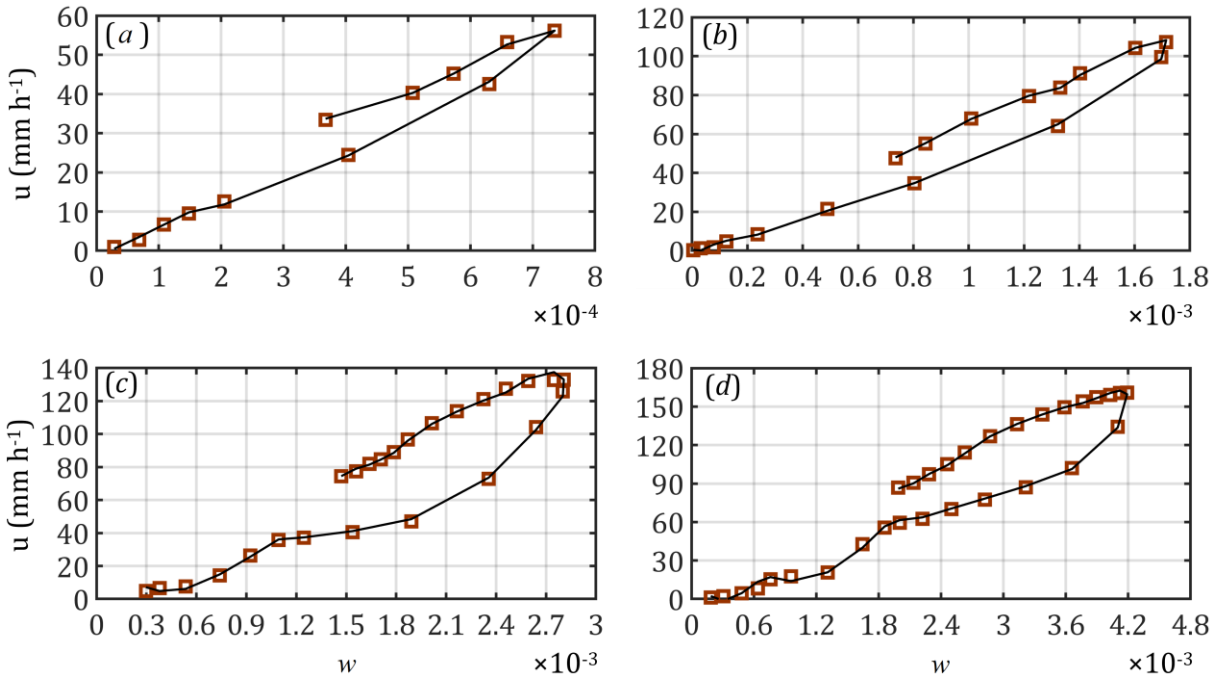

Fig. 7. Modelled and observed water flux exiting the soil column at different rainfall intensities versus soil mobile volumetric water content, for the KDW-VG model. *a*, *b*, *c*, and *d* represent the experiments with rainfall intensities of 56.97, 107.64, 133.01, and 161.71 mm h^{-1}, respectively.

According to Fig. 7, Eq. (15) fit the experimental observations very well, and with very high accuracy. In general, by comparing the results of the two models, (see Tables 1 and 2), it can be concluded that KDW-VG model fit the observations with a slightly lower RMSE value compared to the KDW model. This indicates that the KDW-VG model, in which the power function used in the KDW model was replaced with the van Genuchten model, was able to fit the observations better due to its

564 stronger physical meaning and concept. Generally, the fitting of both KDW and
565 KDW-VG models was better at lower rainfall intensities, because the dispersive
566 effect was gradually decreased with the increase in input intensities. Therefore, the
567 effect of this factor was higher at lower velocities, and fitting of the observations
568 was better at lower rainfall intensities. It should be mentioned that the only
569 common coefficient of the two models, the water dispersion coefficient (ν_w), was
570 found to be almost constant whatever the rainfall intensity and was not affected by
571 the differences between the two models. In addition, Table 2 shows that the
572 changes in the three optimized coefficients of the KDW-VG model are very low
573 regardless of the initial rainfall intensity. This implies that the parameters of the
574 developed KDW-VG model are not sensitive to rainfall intensity, which is one of the
575 advantages of the model developed in this study, whereas, according to Table 1, the
576 coefficient b in the KDW model changed significantly with changes in rainfall
577 intensity.

578 **Comparison of the models' predictions with experimental observations (model**
579 **validation results)**

580 After calibration of the models with data on the water flux exiting the soil column
581 at different rainfall intensities versus soil mobile volumetric water content, the
582 coefficients of both the KDW and KDW-VG models were obtained. These models
583 (Eqs. (7) and (12), respectively) were then solved with a numerical finite difference
584 method. For the numerical solution, the spatial (h) step size of the finite difference
585 method was selected to be equal in all corresponding experiments of both models.

This was also done for temporal (τ) step size. Thereby, the results of the models in corresponding intensities became fairly comparable. These spatial and temporal steps were selected primarily to satisfy the stability condition (see Appendix) and capture the best response of the finite difference method and the lowest RMSE values between observations and the models' predictions. Numerical results were compared to the observed values of the water flux amount exiting the soil column versus time, or the recorded hydrograph at the outlet of the soil column. Figure 8 shows the recorded hydrographs for the different rainfall experiments with different intensities.

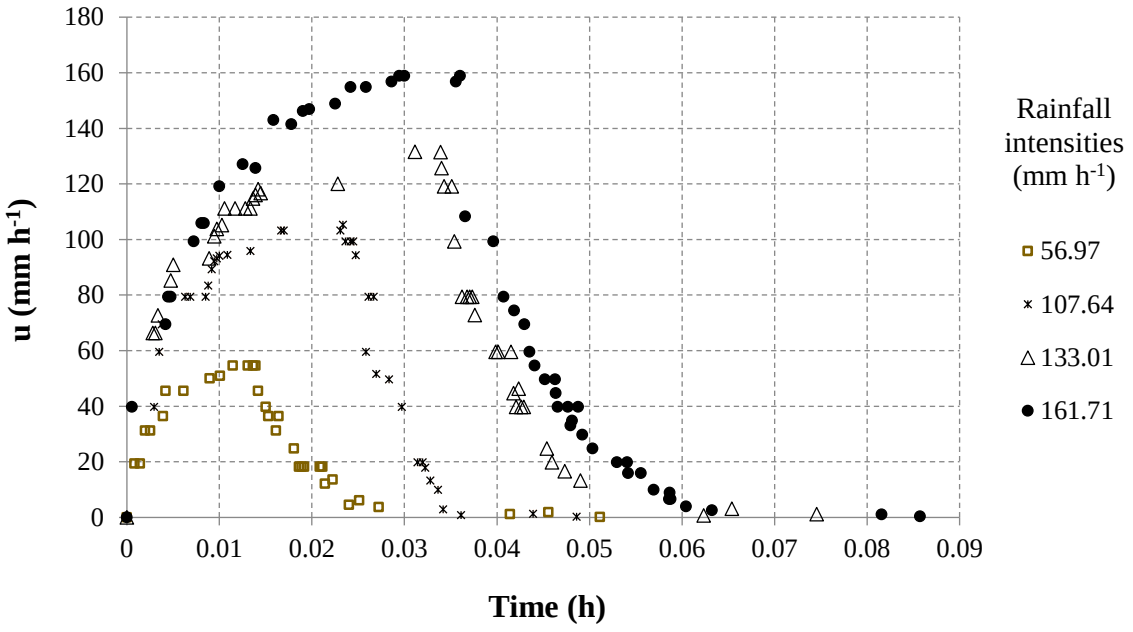

Fig. 8. Output hydrographs from the end of the soil column for different rainfall intensities.

In Fig. 8, regardless of the rainfall intensity, at first, the drainage hydrograph shows a rapid increase in flux u up to a non-sloping part corresponding to a pseudo-steady

599 state, and when the input flow stops, the downside stage is a sudden drop in the
600 flow rate that is followed by a drainage stage with a milder gradient.

601 **Validation of the KDW model**

602 The RMSE between the numerical results and those observed experimentally
603 represents the difference between measurements and simulations. It is shown in
604 Table 3 for different rainfall intensities.

605 **Table 3 RMSE values between the numerical results of the KDW model and the observed values, for**
606 **different rainfall intensities.**

Rainfall intensity (mm h^{-1})	RMSE (mm h^{-1})
56.97	4.34
107.64	7.68
133.01	7.72
161.71	7.20

607

608 The results of this numerical modelling are also displayed in Fig. 9, in which the
609 line represents the simulation results and the circles represent the observed
610 values.

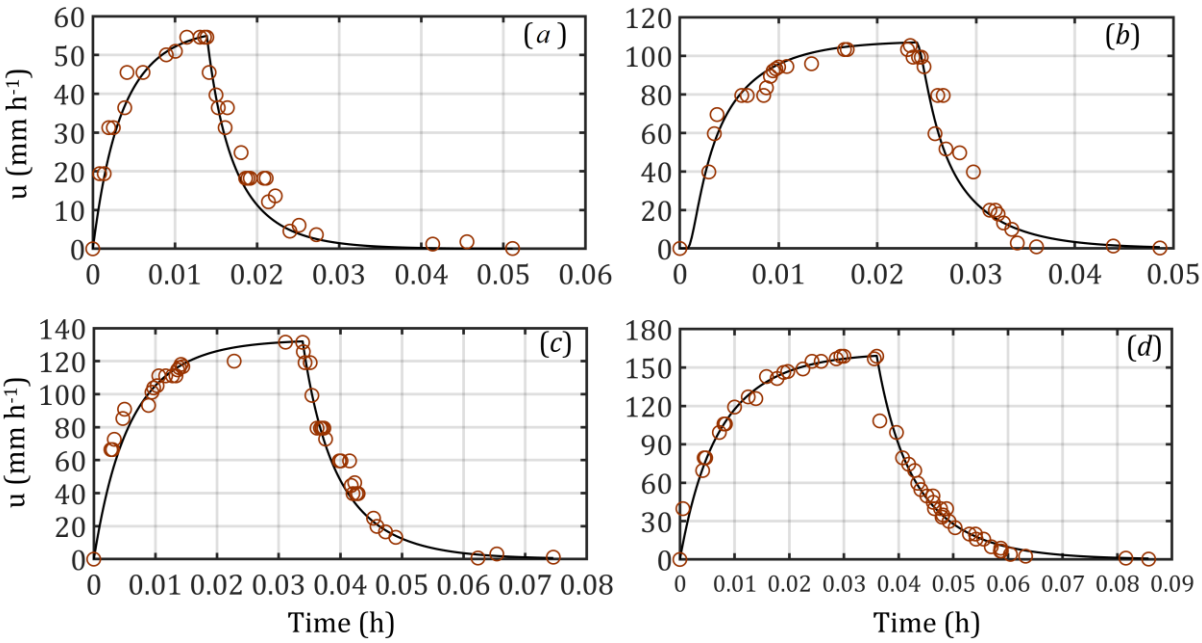

Fig. 9. The numerical results of the KDW model versus the observed values of the experiments for different rainfall intensities. *a*, *b*, *c*, and *d* represent the experiments with rainfall intensities of 56.97, 107.64, 133.01, and161.71 mm h^{-1}, respectively.

As can be seen from Table 3 and Fig. 9, the numerical solutions are in good agreement with experimental observations.

Cross-simulation to determine the optimal coefficients of the KDW model

As discussed earlier, the coefficients of the KDW model were optimized with four different rainfall intensities and the model was calibrated for each. Then, it was important to specify which of these four series of coefficients could be accepted as a single set of coefficients for this soil type whatever the rainfall intensity. To answer the question, as shown in Table 4, the KDW model was separately validated for each rainfall intensity using each series of coefficients, which had separately been calculated previously. Here, the RMSE values for the cross-simulation of the

experiment j (column) were obtained using the estimated parameters from the experiment k (row), which were equal to $k \equiv j = 1, 2, 3, 4$.

Table 4 RMSE values (mm h^{-1}) for cross-simulation of *j* (column) using parameters optimized from the experiment *k* (row) for the KDW model

	Experiments			
Rainfall intensity (mm h^{-1})	56.97	107.64	133.01	161.71
56.97	4.34	12.06	18.07	24.66
107.64	4.50	7.68	12.25	18.53
133.01	6.67	7.32	7.72	10.75
161.71	8.45	11.19	9.51	7.20

As shown in Table 4, the coefficients derived from the rainfall intensity of 133.01 mm h^{-1} gave better predictions of the experimental observations related to the hydrograph of the outlet from the end of the soil column.

Validation of the KDW-VG model

The RMSE values between the numerical results of the KDW-VG model and the observed values of drainage flux are shown for all rainfall intensities in Table 5.

Table 5 RMSE values between the numerical results of the KDW-VG model and the observed values, for different rainfall intensities.

Rainfall intensity (mm h^{-1})	RMSE (mm h^{-1})
56.97	4.29

107.64	7.57
133.01	7.53
161.71	7.09

638

639 The results of this numerical modeling are depicted in Fig. 10 in which the line
640 depicts the simulation results and the circles represent the measurements.

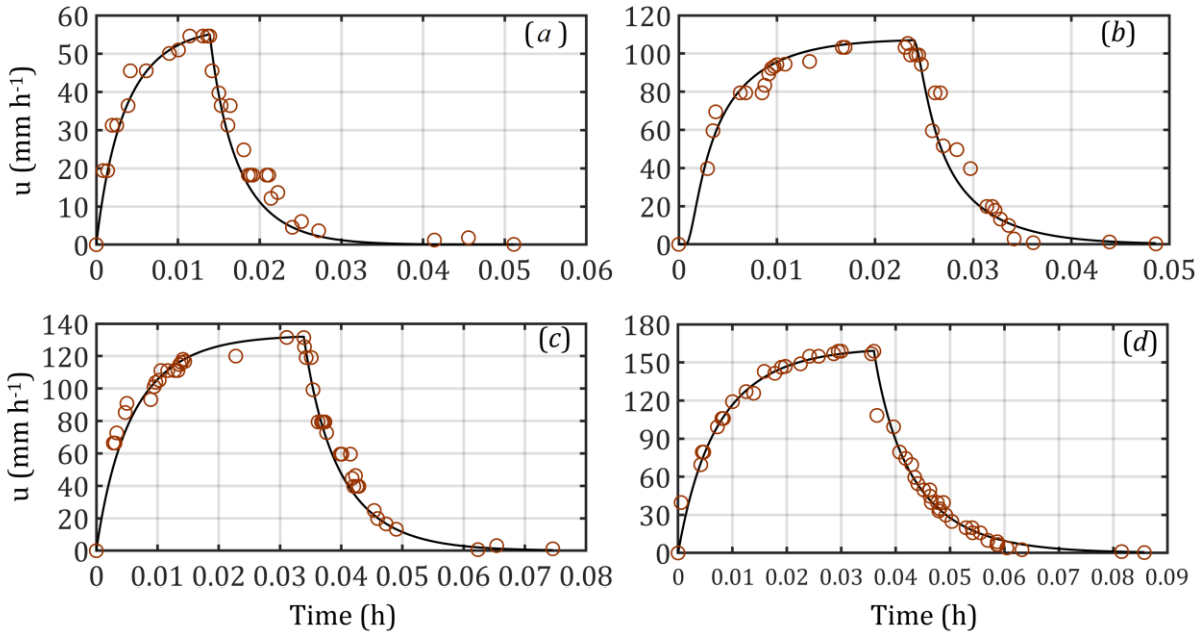

641

642 **Fig. 10. The numerical results of the KDW-VG model versus the observed values of the experiments**
643 **for different rainfall intensities. *a*, *b*, *c*, and *d* represent the experiments with rainfall intensities of**
644 **56.97, 107.64, 133.01, and161.71 mm h^{-1}, respectively.**

645 Based on the results presented in Table 5 and Fig. 10, it is clear that the numerical
646 solutions are strongly consistent with the experimental observations.

647 **Cross-simulation to determine the optimal coefficients of the KDW-VG model**

Here, to determine the best of the four series of coefficients that were separately obtained using each rainfall intensity, as shown in Table 6, the KDW-VG model was separately validated for each level of rainfall intensity using each series of coefficients. As previously, for the cross-simulation of the experiment j (column), the RMSE values were derived from the estimated parameters of the experiment k (row), which were equal to $k \equiv j = 1, 2, 3, 4$, respectively.

Table 6 RMSE values (mm h^{-1}) for cross-simulation of j (column) using parameters optimized from the experiment k (row) for the KDW-VG model.

	Experiments			
Rainfall intensity (mm h^{-1})	56.97	107.64	133.01	161.71
56.97	4.29	7.49	7.77	7.07
107.64	4.37	7.57	8.00	7.11
133.01	4.22	7.38	7.53	7.06
161.71	4.35	7.57	7.91	7.09

As is clear from Table 6, for this model too, the optimized coefficients of rainfall intensity of 131.01 mm h^{-1} provide a better prediction of the experimental observations pertaining to the hydrograph of the outlet from the end of the soil column for all rainfall intensities. However, this prediction for rainfall intensities other than 133.01 mm h^{-1} was better than the prediction of the optimal coefficients of each rainfall intensity, and the third row had the minimum value of RMSE for each column. Here, it should be mentioned that the RMSEs of the prediction of

664 other optimized coefficients for each rainfall intensity were not very different. It
665 can be observed in the columns of Table 6 that the RMSEs of each column are all
666 within the same range and are not very different because, in the KDW-VG model,
667 the coefficients of l, m, and v_w did not differ significantly from one to another
668 irrespective of the rainfall intensity from which they were derived. This is not the
669 case for the original KDW model (see Table 4) and can be seen as one of the
670 advantages of the developed KDW-VG model, for which the input parameters do
671 not depend on the rainfall intensity. In other words, none of the coefficients l, m, or
672 v_w exhibit significant variation in the validation stage when compared with the
673 coefficient b in the KDW model and they could be considered as parameters
674 representative of the soil properties only, whereas the parameters of the KDW
675 models are not representative of the soil properties only as they also depend on
676 the rainfall intensity.

677 **Comparison of performance of the KDW and KDW-VG models in prediction of**
678 **output hydrographs from the end of the soil column**

679 Here, the comparison of Tables 3 and 5 clearly shows that the new KDW-VG model
680 predicted the output hydrograph from the end of the soil column with better
681 accuracy than the original KDW model. In fact, the RMSE values of the KDW-VG
682 model were lower than those of the KDW model for the corresponding rainfall
683 intensities. This finding can also be related to the application of the van Genuchten
684 model, instead of the power equation in the KDW model. The predictions of both
685 the KDW and KDW-VG models were improved at lower rainfall intensities,

686 especially at the rainfall intensity of 56.97 mm h^{-1}. This proves the hypothesis that
687 the dispersive effect is gradually eliminated as input intensities increase, and can
688 be more effective in better prediction at lower velocities. The results show that the
689 dispersion of the wetting front decreases as the input intensity increases. At high
690 intensities, some small-scale dispersive effects, such as capillary effects, may not
691 occur at intermediate pore sizes and the coarse pores, in most cases, participate
692 more in rapid preferential flows. This has also been reported by Di Pietro et al.
693 (2003). Here, for a more accurate comparison of the accuracy of the models, the
694 cumulative square deviations of the measured and predicted values were
695 calculated for both models. The cumulative square deviations are depicted in Fig.
696 11 as a function of time. In Fig. 11, part a shows the shape of the output hydrograph
697 from the end of the soil column for each rainfall intensity, and part b represents the
698 amounts of the cumulative square deviations between the measured and predicted
699 values for both models at the corresponding observation points of part a.

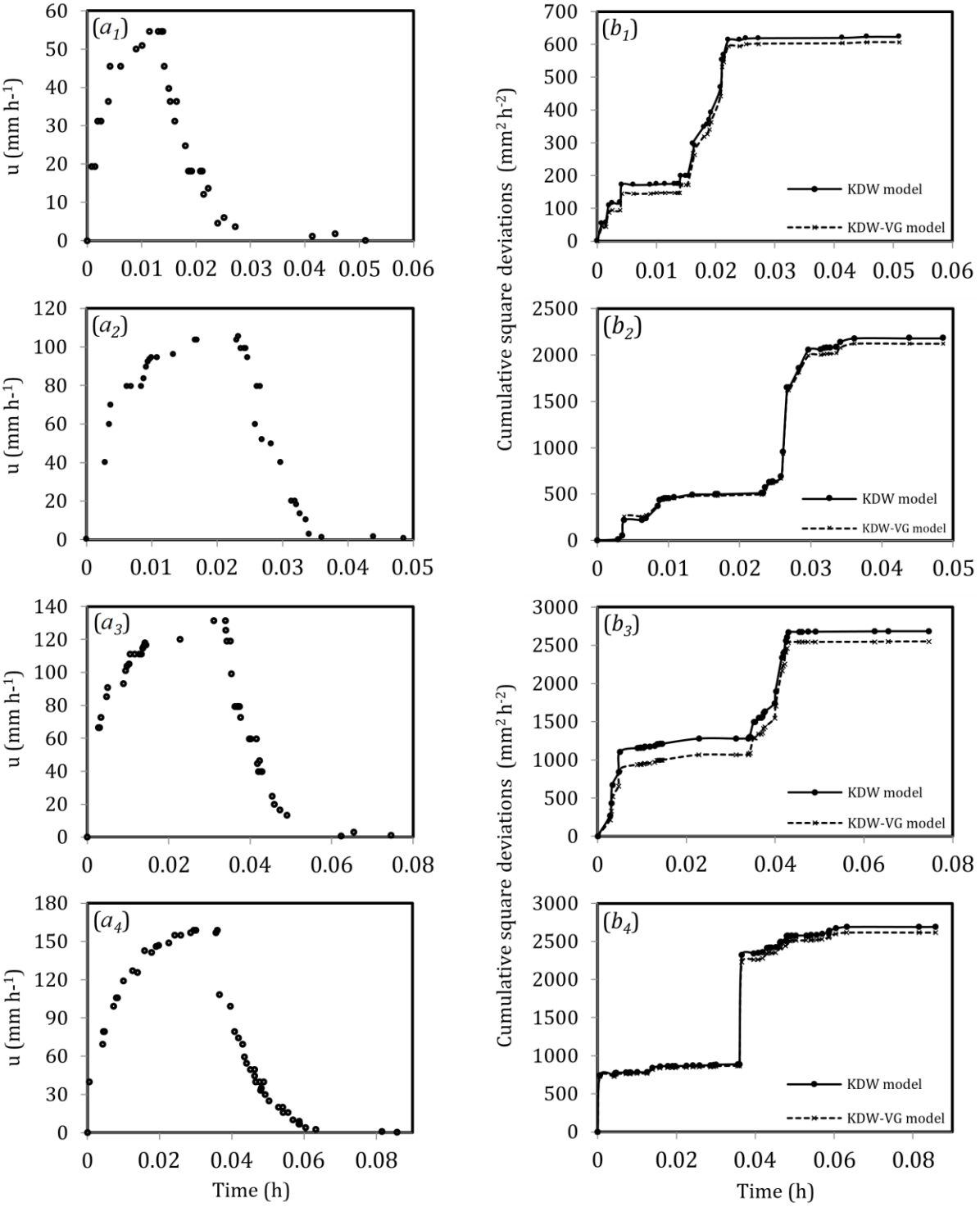

Fig. 11. Output hydrographs from the end of the soil column for different rainfall intensities (a_1~a_4). Cumulative square deviations between the measured and predicted values for both models at the corresponding observation points of part a (b_1~b_4). Numbers 1 to 4 represent the experiments with rainfall intensities of 56.97, 107.64, 133.01, and161.71 mm h^{-1} respectively.

From Fig. 11, it can be seen that the cumulative square deviations between the measured and predicted values versus time are generally lower for the KDW-VG model than for the KDW model. This means that our proposed model is more accurate than the KDW model.

Conclusions

This study presented the new kinematic–dispersive wave van Genuchten (KDW-VG) model for the simulation of water flow through preferential paths. This model is an evolution of the former KDW model (Di Pietro et al., 2003). In the KDW-VG model, the power equation that was applied in the KDW model to describe the relation between water flux and mobile water content was replaced with the shape of the van Genuchten model, which had more physical meaning. Infiltration–drainage experiments were carried out on a soil column prone to preferential flow. A particle swarm optimization (PSO) algorithm was used to optimize and estimate the coefficients of the KDW and KDW-VG models. After parameters optimization, both models could simulate the experiments with very low error. After calibration of the models, the output hydrographs from the end of the soil column were used for validation of the models. Despite a very close agreement between the simulated and measured hydrographs, the KDW-VG model could better predict the drainage hydrograph and water flow through the preferential paths; the RMSE was lower for the KDW-VG model than for the KDW model. The prediction of both models was better at lower rainfall intensities, because when the input rainfall intensities increased, the dispersive effect gradually decreased, and this effect could be more

influential on better prediction processes at lower velocities. Moreover, the optimized parameters of the KDW-VG model were not sensitive to rainfall intensity compared to the coefficients of the KDW model; a single set of parameters representative of only soil properties can be obtained with the KDW-VG model, whereas the KDW parameters also depend on rainfall intensity. This is a very significant advance in the modelling and prediction of preferential flow, but these results need to be confirmed by applying the KDW-VG model for different soils. Overall, the developed equation of this study is suggested to be used in water and solute transport models in porous media, especially to model preferential flows and transport of solutes in soils. For future studies, it is recommended to replace the van Genuchten model with the Burdine (Meng, 2018) or Brooks–Corey models (Huber et al., 2018) to investigate the performance of these models in combination with the KDW model. In addition, for further research work, these experiments could be replicated with a precise weighing lysimeter, to evaluate the efficiency of the KDW-VG model and the solution method and estimate the coefficients for field and real conditions.

Acknowledgements

The corresponding author of this article, Mostafa Moradzadeh, with the permission of the other authors, dedicates this research to the great soul of his mother (Zarin) Kobra Rajabi Foomani to appreciate her devotion as an affectionate mother and conscientious teacher who honestly taught Iranian children for 30 years. Additionally, the authors of the article would like to acknowledge the Iran National

749 Science Foundation (INSF)'s financial support with project No. 94017631. I also
750 thank the Shahid Chamran University of Ahvaz for their cooperation and the
751 provision of experimental equipment.

752 **Appendix**

753 **Numerical solution and discretization**

754 As mentioned, the general form of the partial differential equations used in this
755 study, Eqs. (7) and (12), is as follows:

756 $$\frac{\partial u(z,t)}{\partial t} + c(u)\frac{\partial u(z,t)}{\partial z} = v_u \frac{\partial^2 u(z,t)}{\partial z^2},$$

757 where $v_u = c(u)v_w$.

758 To solve this equation, an explicit scheme is used in spatial and temporal steps. For
759 discretization, with respect to numerical mesh and assuming subscript i for the
760 representation of spatial nodes and subscript j for temporal nodes, the time
761 derivative with a forward difference and the space derivative with a central
762 difference at the j^{th} temporal step were approximated as follows:

763 Time derivative with a forward difference: $$\frac{\partial u}{\partial t} = \frac{u_i^{j+1} - u_i^j}{\tau}$$

764 Space derivative with a central difference: $$\frac{\partial u}{\partial z} = \frac{u_{i+1}^j - u_{i-1}^j}{2h}$$

765 Second-order space derivative: $$\frac{\partial^2 u}{\partial z^2} = \frac{u_{i-1}^j - 2u_i^j + u_{i+1}^j}{h^2}$$

where h is the space interval between the two places and τ is the temporal step. By substituting in the numerical approximations, equivalent to the expressions of the equations used (Eqs. (7) and (12)), the following discretization is derived:

$$\frac{u_i^{j+1}-u_i^j}{\tau} + c(u)\frac{u_{i+1}^j-u_{i-1}^j}{2h} = \nu_w c(u)\frac{u_{i-1}^j-2u_i^j+u_{i+1}^j}{h^2} \quad \text{(A.1)}$$

By arrangement and algebraic displacement of the above equation, the discrete form of the applied models, except for the final nodes is derived as below (according to Fig. A.1):

$$u_i^{j+1} = u_i^j + \frac{\tau v_w}{h^2}c(u)(u_{i-1}^j - 2u_i^j + u_{i+1}^j) - \frac{\tau}{2h}c(u)(u_{i+1}^j - u_{i-1}^j) \quad \text{(A.2)}$$

in which $c(u)$ is the convective celerity, which is a function of u.

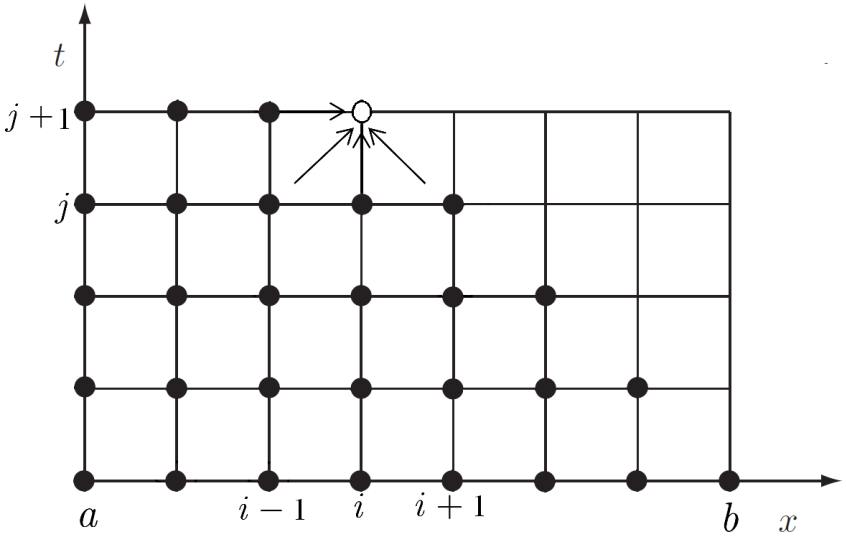

Fig. A.1. Numerical mesh scheme for the numerical solution of Eqs. (7) and (12), except for the final nodes.

For the final nodes, the derivative approximations should not depend on the forward nodes. To do this, the Taylor expansion of f around x_0 is defined as follows:

$$f(x) = f(x_0) + (x - x_0)f'(x_0) + \frac{(x-x_0)^2}{2!}f''(x_0) + \frac{(x-x_0)^3}{3!}f'''(x_0) + \ldots \quad \text{(A.3)}$$

Regarding the above relationship, the following phrases can be written:

$$f(x_0 - 2h) = f(x_0) - 2\,h\,f'(x_0) + 2h^2 f''(x_0) - \frac{4}{3}h^3 f'''(x_0) + \ldots \quad \text{(A.4)}$$

$$f(x_0 - h) = f(x_0) - hf'(x_0) + \frac{h^2}{2!}f''(x_0) - \frac{h^3}{3!}f'''(x_0) + \ldots \quad \text{(A.5)}$$

$$2f(x_0 - h) - f(x_0 - 2h) = f(x_0) - h^2 f''(x_0) + h^3 f'''(x_0) \quad \text{(A.6)}$$

Here, if the phrase $h^3 f'''(x_0)$ is neglected, the second-order derivative approximation of the function f with the order of error of h is obtained as below by algebraic arrangement of the above expression:

$$f''(x_0) = \frac{f(x_0) - 2f(x_0 - h) + f(x_0 - 2h)}{h^2} \Rightarrow \frac{\partial^2 u}{\partial z^2} = \frac{u_i^j - 2u_{i-1}^j + u_{i-2}^j}{h^2} \quad \text{(A.7)}$$

In addition, with the algebraic displacement of Eq. (A.5) and if the $\frac{h^2}{2!}f''(x_0) - \frac{h^3}{3!}f'''(x_0)$ is assumed to be small, the first-order derivative approximation of the function f with the order of error h is as follows:

$$f'(x_0) = \frac{f(x_0) - f(x_0 - h)}{h} \Rightarrow \frac{\partial u}{\partial x} = \frac{u_i^j - u_{i-1}^j}{h} \quad \text{(A.8)}$$

Therefore, the discretization of Eqs. (7) and (12) were approximated as follows for the final nodes with respect to numerical mesh, and assuming subscript i for the

representation of the spatial nodes and subscript j for temporal nodes, the time derivative with a forward difference and the first space derivative with a backward difference in the j^{th} temporal step, and the second-order space derivative based on the discretization of Eq. (A.7):

$$\frac{u_i^{j+1}-u_i^j}{\tau}+c(u)\frac{u_i^j-u_{i-1}^j}{h}=\nu_w c(u)\frac{u_i^j-2u_{i-1}^j+u_{i-2}^j}{h^2} \tag{A.9}$$

With the arrangement and algebraic displacement of the above equation, the discrete form of the applied models is derived for the final nodes as follows (according to Fig. A.2):

$$u_i^{j+1}=u_i^j-\frac{\tau}{h}c(u)(u_i^j-u_{i-1}^j)+\frac{\tau\nu_w}{h^2}c(u)(u_i^j-2u_{i-1}^j+u_{i-2}^j) \tag{A.10}$$

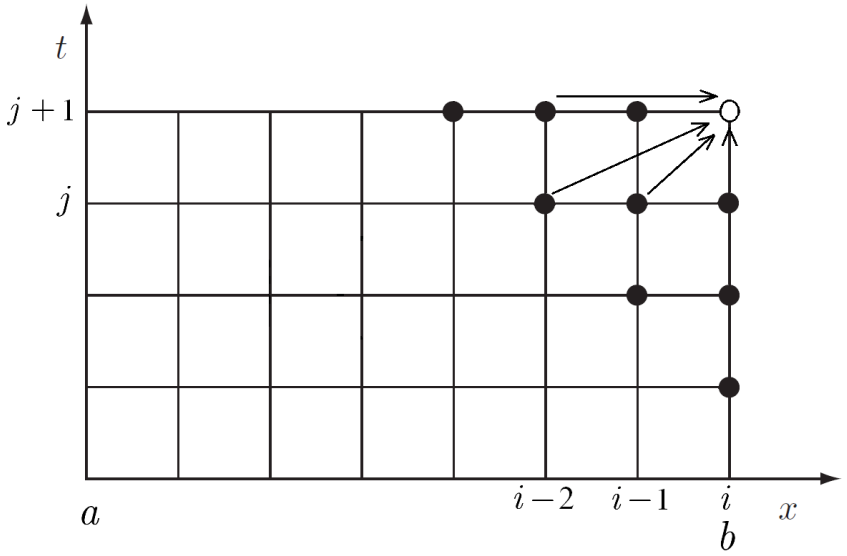

Fig. A.2. Numerical mesh scheme for the numerical solution of Eqs. (7) and (12), for the final nodes.

In addition, h and τ were determined so as to satisfy the following stability condition (Di Pietro et al., 2003), otherwise, the numerical model would not be converged:

$$\left(\left(\frac{\tau}{h}\right)c(u)\right)^2 \le 2\frac{\tau v_w}{h^2}c(u) \le 1 \quad \text{(A.11)}$$

Here, the stability condition is evaluated for $u = u_s$. In the following, the relationship between $c(w)$ and u for the KDW model is expressed as:

$$c(u) = \frac{ab}{b^{\frac{(a-1)}{a}}}[u(z,t)]^{\frac{a-1}{a}} = ab^{\frac{1}{a}}[u(z,t)]^{\frac{a-1}{a}} \quad \text{(A.12)}$$

where u depends on the time and spatial steps of numerical mesh.

Additionally, the wave celerity must be calculated at each temporal step and space interval between the two places. Here, finally, the value of c is considered as follows, accounting for the values of $u_{i-0.5}^{j+0.5}$ (Di Pietro et al., 2003):

$$c(u) = \frac{ab}{b^{\frac{(a-1)}{a}}}\left(\frac{u_i^j + u_{i-1}^{j+1}}{2}\right)^{\frac{(a-1)}{a}} \quad \text{(A.13)}$$

However, for the KDW-VG model, as mentioned previously, the relationship between c and w is as follows:

$$c(w) = \left.\frac{\partial u}{\partial w}\right|_{w_t = constant}$$

$$= \frac{l \times u_{in}(w(z,t) - w_{min})^{l-1}}{(w_{max} - w_{min})^l} \times \left(1 - \left[1 - ({S_e}^*)^{\frac{1}{m}}\right]^m\right)^2$$

$$+ \frac{2u_{in}}{w_{max} - w_{min}}\left(1 - \left[1 - ({S_e}^*)^{\frac{1}{m}}\right]^m\right) \times \left(1 - ({S_e}^*)^{\frac{1}{m}}\right)^{m-1} \times ({S_e}^*)^{\frac{1}{m}+l-1}$$

To determine the relationship between $\boldsymbol{c}$ and $\boldsymbol{u}$, $\boldsymbol{w}$ must first be arranged according to $\boldsymbol{u}$. To do this, based on the water flux experiments ($\boldsymbol{u}$) versus mobile water content ($\boldsymbol{w}$), a polynomial or exponential equation was obtained as $\boldsymbol{w} = \boldsymbol{f}(\boldsymbol{u})$

according to the experiments and for each rainfall intensity. Subsequently, this equation derived from the experiments was used instead of the $\boldsymbol{w}(\boldsymbol{z},\boldsymbol{t})$ value in the above equation. Thus, $\boldsymbol{c}(\boldsymbol{u})$ was determined for each experiment. Here, the value of $\boldsymbol{c}$ was again considered as $\left(\boldsymbol{u}_{\boldsymbol{i}}^{\boldsymbol{j}}+\boldsymbol{u}_{\boldsymbol{i-1}}^{\boldsymbol{j+1}}\right)/\mathbf{2}$, accounting for the values of $\boldsymbol{u}_{\boldsymbol{i-0.5}}^{\boldsymbol{j+0.5}}$.

References

1. Abbasi, F., Javaux, M., Vanclooster, M., Feyen, J., 2012. Estimating hysteresis in the soil water retention curve from monolith experiments. Geoderma. 189, 480-490.
2. Ajdad, H., Baba, Y.F., Al Mers, A., Merroun, O., Bouatem, A., Boutammachte, N., 2019. Particle swarm optimization algorithm for Optical-geometric optimization of Linear Fresnel solar concentrators. Renew. Energ. 130, 992-1001.
3. Alaoui, A., 2015. Modelling susceptibility of grassland soil to macropore flow. J. Hydrol. 525, 536-546.
4. Banks, A., Vincent, J., Anyakoha, C., 2008. A review of particle swarm optimization. Part II: hybridisation, combinatorial, multicriteria and constrained optimization, and indicative applications. Nat. Comput. 7(1), pp.109-124.
5. Bansal, J.C., Singh, P.K., Saraswat, M., Verma, A., Jadon, S.S., Abraham, A., 2011, October. Inertia weight strategies in particle swarm optimization. In Nature and Biologically Inspired Computing (NaBIC), 2011 Third World Congress on (pp. 633-640). IEEE.
6. Carsel, R.F., Parrish, R.S., 1988. Developing joint probability distributions of soil water retention characteristics. Water. Resour. Res. 24(5), 755-769.
7. Chen, C., Wagenet, R.J., 1992. Simulation of water and chemicals in macropore soils Part 1. Representation of the equivalent macropore influence and its effect on soil water flow. J. Hydrol. 130(1-4), 105-126.
8. Chen, K., Zhou, F.Y., Yin, L., Wang, S.Q., Wang, Y.G., Wan, F., 2018. A hybrid particle swarm optimizer with sine cosine acceleration coefficients. Inform. Sciences. 422, 218-241.
9. Cohen, M., Weisbrod, N., 2018. Transport of iron nanoparticles through natural discrete fractures. Water. Res. 129, 375-383.

10. Di Pietro, L., Lafolie, F., 1991. Water flow characterization and test of a kinematic-wave model for macropore flow in a highly contrasted and irregular double-porosi medium. J. Soil .Sci. 42(4), pp.551-563.
11. Di Pietro, L., Ruy, S., Capowiez, Y., 2003. Predicting preferential water flow in soils by traveling-dispersive waves. J. Hydrol. 278(1), 64-75.
12. Eberhart, R.C., Shi, Y., 2001. Tracking and optimizing dynamic systems with particle swarms. In Evolutionary Computation, 2001. Proceedings of the 2001 Congress on (Vol. 1, pp. 94-100). IEEE.
13. Feng, Y., Teng, G.F., Wang, A.X., Yao, Y.M., 2007, September. Chaotic inertia weight in particle swarm optimization. In Innovative Computing, Information and Control, 2007. ICICIC'07. Second International Conference on (pp. 475-475). IEEE.
14. Flury, M., 1996. Experimental evidence of transport of pesticides through field soils- a review. J. Environ. Qual. 25(1), 25-45.
15. Gallage, C., Kodikara, J., Uchimura, T., 2013. Laboratory measurement of hydraulic conductivity functions of two unsaturated sandy soils during drying and wetting processes. Soils. Found. 53(3), 417-430.
16. Gerke, H.H., 2006. Preferential flow descriptions for structured soils. J. Plant. Nutr. Soil. Sc. 169(3), 382-400.
17. Germann, P.F., 1985. Kinematic wave approach to infiltration and drainage into and from soil macropores. T. ASAE. 28(3), 745-0749.
18. Germann, P.F., 1990. Preferential flow and the generation of runoff: 1. Boundary layer flow theory. Water. Resour. Res. 26(12), 3055-3063.

19. Ghanbarian-Alavijeh, B., Liaghat, A., Huang, G.H., Van Genuchten, M.T., 2010. Estimation of the van Genuchten soil water retention properties from soil textural data. Pedosphere. 20(4), 456-465.
20. Hoffman, F., Ronen, D. and Pearl, Z., 1996. Evaluation of flow characteristics of a sand column using magnetic resonance imaging. J. Contam. Hydrol., 22(1-2), pp.95-107.
21. Huber, E., Stroock, A., Koch, D., 2018, Modeling the Dynamics of Remobilized CO2 within the Geologic Subsurface. Int. J. Greenh. Gas. Con. 70: 128–145.
22. Jarvis, N.J., 2007. A review of non-equilibrium water flow and solute transport in soil macropores: Principles, controlling factors and consequences for water quality. Eur. J. Soil. Sci. 58(3), 523-546.
23. Kennedy, J., Eberhart, R.C., 1995. Particle Swarm Optimization. In Proceedings of IEEE International Conference on Neural Networks, Perth, Australia, IEEE Service Center, Piscataway, NJ, Vol. IV, 1942-1948.
24. Kentzoglanakis, K., Poole, M., 2009, July. Particle swarm optimization with an oscillating inertia weight. In Proceedings of the 11th Annual conference on Genetic and evolutionary computation (pp. 1749-1750). ACM.
25. Khitrov, N.B., Zeiliger, A.M., Goryutkina, N.V., Omel'chenko, N.P., Nikitina, N.S. Utkaeva, V.F., 2009. Preferential water flows in an ordinary chernozem of the Azov Plain. Eurasian. Soil. Sci. 42(7), 757-768.
26. Klammler, H., Layton, L., Nemer, B., Hatfield, K., Mohseni, A., 2017. Theoretical aspects for estimating anisotropic saturated hydraulic conductivity from in-well or direct-push probe injection tests in uniform media. Adv. Water. Resour. 104, 242-254.

27. Leij, F.J., Alves, W.J., Van Genuchten, M.T., Williams, J.R., 1996. Unsaturated soil hydraulic database, UNSODA 1.0 user's manual. Rep (Vol. 96). EPA/600.

28. Li, B.T., Pales, A.R., Clifford, H.M., Kupis, S., Hennessy, S., Liang, W.Z., Moysey, S., Powell, B., Finneran, K.T., Darnault, C.J., 2018. Preferential Flow in the Vadose Zone and Interface Dynamics: Impact of Microbial Exudates. J. Hydrol. 558, 72-89.

29. Li, H.R., Gao, Y.L., 2009, May. Particle swarm optimization algorithm with exponent decreasing inertia weight and stochastic mutation. In Information and Computing Science, 2009. ICIC'09. Second International Conference on (Vol. 1, pp. 66-69). IEEE.

30. Majdalani, S., Angulo-Jaramillo, R., Di Pietro, L., 2008. Estimating preferential water flow parameters using a binary genetic algorithm inverse method. Environ. Modell. Softw. 23(7), 950-956.

31. Malik, R.F., Rahman, T.A., Hashim, S.Z.M., Ngah, R., 2007. New particle swarm optimizer with sigmoid increasing inertia weight. Int. J. Comput. Sci. Secur. 1(2), 35-44.

32. Meng, H., 2018. Study on the rock-electric and the relative permeability characteristics in porous rocks based on the curved cylinder-sphere model. J. Petrol. Sci. Eng. 166, 891-899.

33. Moradzadeh, M., Moazed, H., Sayyad, G., Khaledian, M., 2014. Transport of nitrate and ammonium ions in a sandy loam soil treated with potassium zeolite–Evaluating equilibrium and non-equilibrium equations. Acta. Ecol. Sinica. 34(6), 342-350.

34. Mualem, Y., 1976. A new model for predicting the hydraulic conductivity of unsaturated porous media. Water. Resour. Res. 12(3), pp.513-522.

35. Nielsen, D.R., Biggar, J.W., 1961. Measuring capillary conductivity. Soil. Sci. 92(3), 192-193.

921 36. Nikabadi, A., Ebadzadeh, M., 2008. Particle swarm optimization algorithms with adaptive
922 Inertia Weight: A survey of the state of the art and a Novel method. IEEE J. Evol. Computat.
923 37. Niu, J.Z., Yu, X.X., Zhang, Z.Q., 2007. Soil preferential flow in the dark coniferous forest of
924 Gongga Mountain based on the kinetic wave model with dispersion wave (KDW
925 preferential flow model). Acta. Ecol. Sinica. 27(9), 3541-3555.
926 38. Poulovassilis, A., 1969. The effect of hysteresis of pore-water on the hydraulic
927 conductivity. Eur. J. Soil. Sci. 20(1), 52-56.
928 39. Radcliffe, D.E. and Simunek, J., 2010. Soil physics with HYDRUS: Modeling and
929 applications. CRC press.
930 40. Rauch, W., Harremoës, P., 1999. On the potential of genetic algorithms in urban drainage
931 modeling. Urban Water, 1(1), 79-89.
932 41. Saadat, S., Bowling, L., Frankenberger, J., Kladivko, E., 2018. Nitrate and phosphorus
933 transport through subsurface drains under free and controlled drainage. Water. Res. 142,
934 196-207.
935 42. Salahi, M., Jamalian, A., Taati, A., 2013. Global minimization of multi-funnel functions
936 using particle swarm optimization. Neural. Comput. Appl. 23(7-8), 2101-2106.
937 43. Sander, T. and Gerke, H.H., 2007. Preferential flow patterns in paddy fields using a dye
938 tracer. Vadose. Zone. J., 6(1), pp.105-115.
939 44. Schaap, M.G., Leij, F.J., Van Genuchten, M.T., 2001. Rosetta: A computer program for
940 estimating soil hydraulic parameters with hierarchical pedotransfer functions. J. Hydrol.
941 251(3-4), 163-176.

942 45. Sheng, F., Wang, K., Zhang, R.D., Liu, H.H., 2011. Modeling preferential water flow and
943 solute transport in unsaturated soil using the active region model. Environ. Earth. Sci.
944 62(7), 1491-1501.
945 46. Shi, Y.H., Eberhart, R., 1998, May. A modified particle swarm optimizer. In Evolutionary
946 Computation Proceedings, 1998. IEEE World Congress on Computational Intelligence,
947 The 1998 IEEE International Conference on (pp. 69-73). IEEE.
948 47. Snehota, M., Jelinkova, V., Sacha, J., Frycova, M., Cislerova, M., Vontobel, P., Hovind, J., 2015.
949 Experimental investigation of preferential flow in a near-saturated intact soil sample.
950 Physcs. Proc. 69, 496-502.
951 48. Tao, Y., He, Y.B., Duan, X.Q., Zou, Z.Q., Lin, L.R., Chen, J.Z., 2017. Preferential flows and soil
952 moistures on a Benggang slope: Determined by the water and temperature co-
953 monitoring. J. Hydrol. 553, 678-690.
954 49. Topp, G.C., Miller, E.E., 1966. Hysteretic Moisture Characteristics and Hydraulic
955 Conductivities for Glass-Bead Media1. Soil. Sci. Soc. Am. J. 30(2), 156-162.
956 50. Tsoulos, I.G., Stavrakoudis, A., 2010. Enhancing PSO methods for global optimization.
957 Appl. Math. Comput. 216(10), 2988-3001.
958 51. van Genuchten, M.T., 1980. A closed-form equation for predicting the hydraulic
959 conductivity of unsaturated soils. Soil. Sci. Soc. Am. J. 44(5), .892-898.
960 52. Wang, Y.Q., Ma, J.Z., Guan, H.D., Zhu, G.F., 2017. Determination of the saturated film
961 conductivity to improve the EMFX model in describing the soil hydraulic properties over
962 the entire moisture range. J. Hydrol. 549, 38-49.

963 53. Wang, Y.S., Bradford, S.A., Šimůnek, J., 2013. Transport and fate of microorganisms in soils
964 with preferential flow under different solution chemistry conditions. Water. Resour. Res.
965 49(5), 2424-2436.
966 54. Wang, Y.S., Bradford, S.A., Šimůnek, J., 2014. Physical and chemical factors influencing the
967 transport and fate of E. coli D21g in soils with preferential flow. Vadose. Zone. J., 13.
968 55. Xin, J.B., Chen, G.M., Hai, Y.B., 2009, April. A particle swarm optimizer with multi-stage
969 linearly-decreasing inertia weight. In Computational Sciences and Optimization, 2009.
970 CSO 2009. International Joint Conference on (Vol. 1, pp. 505-508). IEEE.
971 56. Yan, Y.T., Zhang, R., Wang, J., Li, J.M., 2018. Modified PSO algorithms with "Request and
972 Reset" for leak source localization using multiple robots. Neurocomputing, 292, 82-90.
973 57. Yates, S.R., Van Genuchten, M.T., Leij, F.J., Warrick, A.W., 1992. Analysis of measured,
974 predicted, and estimated hydraulic conductivity using the RETC computer program. Soil.
975 Sci. Soc. Am. J. 56(2), 347-354.
976 58. Youngs, E.G., 1964. An Infiltration Method of Measuring the Hydraulic Conductivity of
977 Unsaturated Porous Materials. Soil. Sci. 97(5), 307-311.
978 59. Zhang, J., Lei, T.W., Qu, L.Q., Chen, P., Gao, X.F., Chen, C., Yuan, L.L., Zhang, M.L., Su, G.X.,
979 2017. Method to measure soil matrix infiltration in forest soil. J. Hydrol. 552, 241-248.
980 60. Zhang, Z.B., Peng, X., Zhou, H., Lin, H., Sun, H., 2015. Characterizing preferential flow in
981 cracked paddy soils using computed tomography and breakthrough curve. Soil. Till. Res.
982 146, 53-65.